jnm/INSTRUMENTATION AND PHYSICS

Design and Performance Characteristics of a Whole-Body Positron Transaxial Tomograph

Edward J. Hoffman, Michael E. Phelps,* Nizar A. Mullani,
Carol S. Higgins, and Michel M. Ter-Pogossian

Washington University School of Medicine, St. Louis, Missouri

A whole-body positron-emission transaxial tomograph (PETT III) is described in detail and evaluated in terms of resolution, accuracy, and efficiency. The PETT III utilizes annihilation coincidence detection to provide spatial resolution; high sensitivity is achieved by using 48 NaI(Tl) detectors set in a hexagonal array with a multiple-coincidence logic. The assumptions and approximations made in the reconstruction and their effect on image quality are discussed. Phantom studies show the depth-independent resolution and response of PETT III, as well as its ability to recover activity distribution quantitatively in the cross section measured. Images obtained with patients and normal volunteers show the potential clinical utility of PETT III.

J Nucl Med 17: 493–502, 1976

We have designed, built, and tested a device that allows the reconstruction of transaxial tomographic images of the distribution of positron-emitting radiopharmaceuticals in the human head and torso. This is the third in a series of devices (the first two being prototypes) that we call positron-emission transaxial tomographs (PETT). The PETT III can measure quantitatively the distribution of any positron-emitting radiopharmaceutical in a cross-sectional slice of the human body. The design of PETT III is based on the principles discussed in Refs. *1–4*. The application of positron-emitting radiopharmaceuticals in transaxial tomography are also studied in Refs. *5–9*. This paper presents (A) a description of a clinically useful PETT; (B) a report on its capabilities in terms of resolution, accuracy, and efficiency; and (C) documentation of the imaging capability of PETT III with both patients and volunteers.

DESCRIPTION OF PETT III

The basic measurement of transaxial tomography consists of a set of rectilinear scans for a set of angles about a cross section of an object. In order to obtain these measurements efficiently, PETT III employs 48 NaI(Tl) scintillation detectors placed about a cross section in a hexagonal array. Six sets of eight detectors are each mounted on platforms capable of rectilinear motion; the six platforms of detectors are mounted on a gantry that provides a rotational motion. A photograph of PETT III is shown in Fig. 1. To provide spatial resolution, this system utilizes coincidence counting of positron annihilation radiation (*1,2,4*) instead of lead collimators. In order to maximize the sensitivity of the system, each detector is in coincidence with all of the detectors on the opposite bank. Figure 2 shows a schematic layout of the PETT III system, indicating the multiple-coincidence scheme.

The PETT III was designed to have flexibility both in terms of linear and angular sampling frequency and in terms of the spatial resolution of the detection system. The linear motion of the detector platforms and the rotational motion of the gantry are controlled by stepping motors, which allow a wide range in the choice of linear and angular sampling increments. The spatial resolution of the detectors is determined by lead shadow shields and can be varied by using different sets of shields (*1,2*). The PETT III

Received Aug. 20, 1975; revision accepted Nov. 26, 1975.

For reprints contact: E. J. Hoffman, Dept. of Radiology, Hospital of the University of Pennsylvania, 3400 Spruce St., Philadelphia, Pa. 19104.

* Present address: Dept. of Radiology, Hospital of the University of Pennsylvania, 3400 Spruce St., Philadelphia, Pa. 19104.

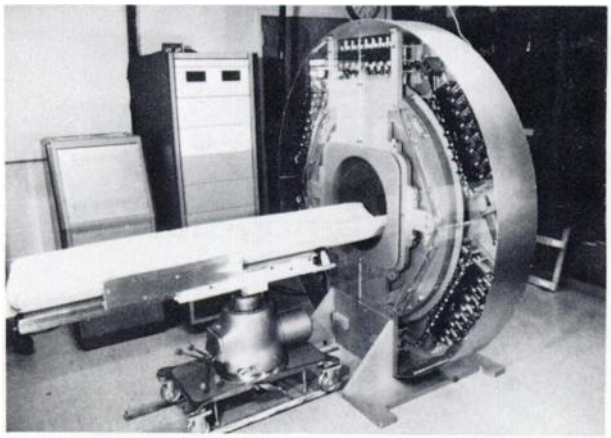

FIG. 1. Photograph of PETT III. Coincidence circuitry and computer interface are contained in cabinet to right. Power supplies for stepping motors are in left cabinet. System computer is in adjacent room.

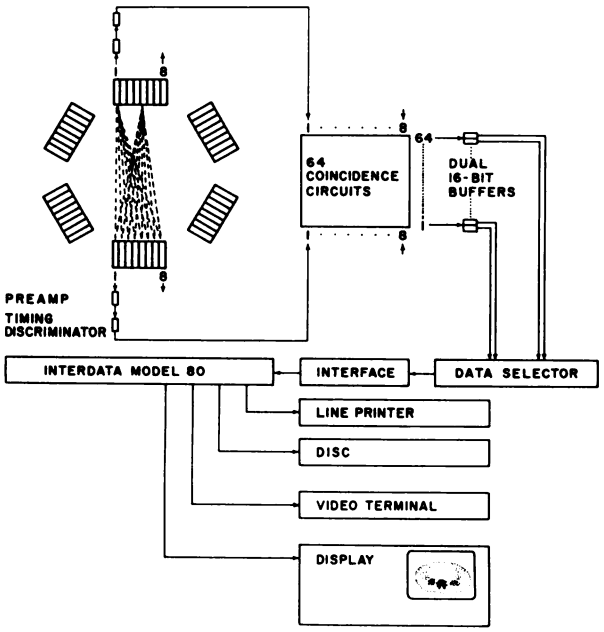

FIG. 2. Block diagram for PETT III shows layout of detectors with illustrative lines of response for multiple-coincidence scheme.

was also designed to exhibit a uniform detection response as a function of the depth between each pair of coincident detectors. These design criteria allow the system to image over a wide range of injected activities and should provide confidence that the image reconstructed from the collected data represents the true distribution of activity.

PHYSICAL DESCRIPTION

With covers in place, PETT III is 192 cm high and 192 cm wide, with a patient port that is 51 cm in diameter and 34 cm deep. The distance between opposing banks of detectors has been set at 111.2 cm. The total field of view of the device is a circle 48 cm in diameter.

The placement of the 48 detectors with respect to the patient and to each other is critical and was determined from a combination of interacting factors. In the first approximation, the detector positions were dictated by the need for uniformity of detection response with depth within the field of view, by the counting efficiency of the detectors, and by the proposed size of the field of view. The exact placement of the detectors was dictated by the geometric positions of their lines of response and the requirements of the reconstruction algorithm for sets of data derived from parallel lines of response.

After testing several detector sizes it was decided that in terms of efficiency, cost, and resolution [2.1 cm full width at half maximum (FWHM)] for the completely exposed detector pairs, a NaI(Tl) detector 5.08 cm in diameter by 7.62 cm long would be optimal. Since the system was to take sections in the torso, a uniform detector response over a 40–50-cm region was desirable. Measurement of the line spread functions (LSF) as a function of depth for various detector separations indicated that a detector-to-detector distance of about 100 cm would be required. With a field size of about 50 cm, eight detectors on a bank with center-to-center spacing of 6 cm would be required. With the above requirements, the highest packing density of crystals in a regular polygon in a plane is obtained with a hexagonal array.

The position of the detectors is dictated primarily by the reconstruction algorithm. The input data for the calculation are sets of rectilinear activity profiles, sampled at regularly spaced intervals and measured at regularly spaced angles. These requirements are easily achieved by a system in which only those detectors directly opposite each other are in coincidence, but in PETT III each detector is in coincidence with all of the detectors on the opposite bank. In this multiple-coincidence scheme, data are taken simultaneously for several angles at each angular position during a scan. If the positions of the detectors are not carefully chosen, some data will fall at odd angles or will coincide poorly with the angle of the other data in the activity profile in which they are placed. These problems would lead to information loss if such data are rejected or to image distortion if they are accepted.

The solution to the angulation problem in PETT III is illustrated in Fig. 3. Here two angular positions of a hexagonal detector array are shown: Position 1 is represented by solid lines and Position 2 by dashed

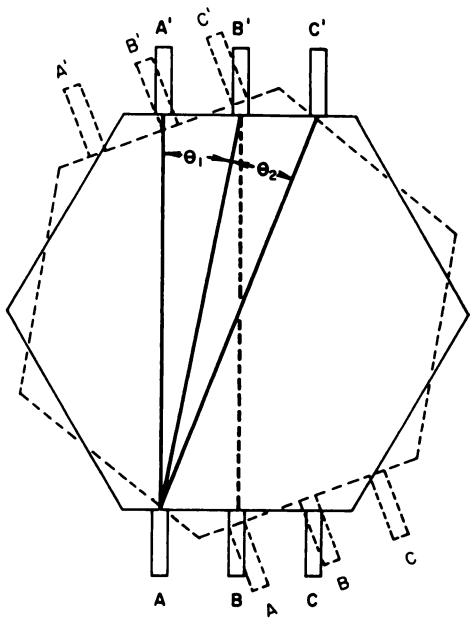

FIG. 3. Illustration of geometric property utilized in PETT III to allow easy sorting of data into activity profiles. Every coincident line of response (e.g., A–C′) not with directly opposing detector (e.g., B–B′) will fall on line corresponding to directly opposing pair at another angular position.

lines. The ideal situation is illustrated by the rotation. In Position 1 there is a line of response between detectors B and B′, and if the hexagon is rotated to Position 2, detectors A and C′ will view the same line. The PETT III is designed in such a way that this type of superposition occurs for every line of response at every angle in the completed scan. In order to accomplish this, three conditions must be met. The first condition is that all angles (e.g., θ_1 and θ_2 in Fig. 3) formed by a detector on one bank and two neighboring detectors on the opposite bank, should be equal. This can be accomplished if θ is small. The second condition is that the angle Φ, the total angle subtended at one detector by all the detectors on the opposite bank, must not be too large. For example, Φ must still be nearly proportional to its own tangent. The third condition is that the total angle of rotation of the instrument should be an integral multiple of θ.

In PETT III the first condition is satisfied by making θ equal to 3°. By rotating 3° or some multiple of 3° per angular step, there will be superposition of data, as seen in Fig. 3. The second condition is satisfied if $\Phi = 21°$. On PETT III the actual tan Φ is 0.378, while tan 21° = 0.383, which is within 2%. The PETT III rotates only 60° (additional rotation would be redundant), and since this rotation is an integral multiple of 3°, the third condition is satisfied.

With this multiple-coincidence scheme, each line of response falls on other lines of response, with the net effect of redundant sampling throughout the cross section. One result of this arrangement is that the central region of the field of view of PETT III is viewed more efficiently than the peripheral regions. Figure 2 shows how the density of the lines of response increases toward the center. This nonuniform sampling may appear undesirable, but actually it is a very useful property in that the gamma photon attenuation is highest along lines through the center of a body and the increased sampling in the center improves the statistical quality of the data in the center, where the count rate per unit area would tend to be lowest (*10*).

Although the spatial resolution of PETT III is not determined by lead collimators, shielding for the detectors is critical for optimal performance. The lead shielding in the system is designed to protect the detectors from radiation originating in parts of the patient's body outside the field of interest; the shield reduces accidental coincidences to an acceptable level. Most of the shielding is provided by two stationary disks of lead on each side of the measurement plane. These shields have a 60-cm hole to accommodate the patient and the bearings on which the gantry rotates. The shields are 2.54 cm thick out to a 100 cm diameter and 5.08 cm thick out to a 128 cm diameter. In addition, two lead rings with 60 cm inner diameter and 65 cm outer diameter are mounted on the gantry to provide a slit shield, which only permits the detectors to be exposed to a slice of the patient 2.5 cm thick.

Removable shadow shields are employed in PETT III to define the inherent spatial resolution of the system. The shadow shields are 2.54-cm-thick lead plates, placed between the patient and the detectors, with holes over the center of each detector. The spatial resolution in terms of FWHM of LSFs is approximately 40% of the diameter of these holes (*1,2*). Currently the shadow shields have 2.54-cm-diam holes that are flared to allow each detector an unobstructed view of all the detectors on the opposite bank.

The detectors are held in position in a 50 × 6.5 × 7.5-cm lead block with holes for the detectors. There is a minimum of 3 mm of lead between adjacent detectors. This holder reduces detector-to-detector scatter from 5% for an unshielded pair of neighboring detectors to less than 0.5% with the shielding.

DETECTORS AND ELECTRONICS

The detectors used in PETT III are 5.08 × 7.62-cm NaI(Tl) scintillation detectors (Bicron Model 2M3/2). The anode signal from each detector is

TABLE 1. RESOLUTION OF COINCIDENT DETECTOR PAIRS AS A FUNCTION OF Ψ WITH SHADOW SHIELDS IN PLACE

	Photopeak only		Discriminator set at 100 keV	
Ψ (deg)	FWHM (cm)	FWTM (cm)	FWHM (cm)	FWTM (cm)
0	1.20	2.15	1.30	2.30
3	1.20	2.20	1.30	2.35
6	1.15	2.25	1.30	2.40
9	1.10	2.20	1.25	2.40
12	1.10	2.15	1.15	2.35
15	1.05	2.15	1.15	2.25
18	1.00	2.15	1.15	2.30
21	0.95	2.10	1.10	2.15

TABLE 2. RESOLUTION OF COINCIDENT DETECTOR PAIRS AS A FUNCTION OF Ψ WITHOUT SHADOW SHIELDS

	Photopeak only		Discriminator set at 100 keV	
Ψ (deg)	FWHM (cm)	FWTM (cm)	FWHM (cm)	FWTM (cm)
0	2.10	3.75	2.25	4.15
3	2.15	3.85	2.40	4.15
6	2.10	3.85	2.40	4.35
9	2.10	3.70	2.30	4.20
12	2.05	3.70	2.20	4.15
15	2.00	3.70	2.15	4.10
18	2.00	3.65	2.25	4.15
21	2.00	3.80	2.10	4.05

amplified by a factor of 10 with an Ortec Model-9301 fast preamplifier. This signal is then sent to an EG&G/Ortec Model-T308/NL octal discriminator, which provides a variable level of energy discrimination and an output signal of variable width suitable for fast timing.

The eight outputs from each detector bank are sent to one octal discriminator. The timing signals from opposing banks of detectors are sent to an 8×8 matrix of coincidence gates. Each gate is followed by a 1-bit latch that is set with each coincidence and reset by the counting circuitry when interrogated. During the operation of PETT III the counting control circuits continuously interrogate and reset the latches and update a 64-word 16-bit-per-word counter memory. There are three sets of such coincidence and counter circuitry, one for each pair of opposed detector banks. Data loss caused by this circuitry is less than 0.1% at 150 coincidence counts per detector pair per second. In order to allow phasic data collection, a second memory bank was built into the interface so that the data can be channeled into either memory bank in accordance with some criterion, such as the systolic and diastolic phases of the cardiac cycle. Data are transferred to the computer only after a specified integration period, thereby freeing most of the computer time for data processing.

Control logic for scanning motion. This logic controls the transverse and rotational motion of the detector assemblies. It consists of three registers, set under computer control, that are responsible for the number of pulses sent to the stepping motors. The PETT III has seven stepping motors, one for the rectilinear motion of each bank of detectors and one for the rotation of the gantry.

When the preset time interval is finished, a signal is sent from the computer to the motion control logic, which then moves the detector arrays to the next scan position. Two micro switches are incorporated with each detector assembly and the rotation gear to limit the total distance traveled to each extreme point. The system is capable of rectilinear motion of 1 cm/sec and can rotate at 3°/sec, assuming a minimum scan time of about 2 min for 3° angular increments.

Computer system. The computer utilized in PETT III is an Interdata Model 80. This is a 16-bit computer with an approximately 350-nsec cycle time; it includes floating-point hardware and has 32 kilobytes of memory. Peripherals include two Diablo Model-33 moveable head disks for mass data storage, a nine-track 800-bits/in. industry-compatible magnetic tape drive for archival storage (Bucode Model 4025), and a Ramtek 256×256 video display system capable of producing 64 levels of gray. A block diagram of the system is included in Fig. 2.

PETT III software. The data handling for PETT III may be divided logically into four stages: (A) acquisition, (B) correction and sorting, (C) reconstruction, and (D) image display. Data collection is controlled by an assembly language program that allows for selection of integration time, angular increment, and number of transverse positions. At present, data are generally collected every 3° with six transverse positions at each angle. During collection, data are presorted according to detector bank and coincidence line of response and stored as 16-bit integers on either a 2.5-megabyte disk or a nine-track magnetic tape.

Following data acquisition, corrections are made for radioactive decay and detection nonuniformity (*1,2*). The data are then sorted into 60 profiles containing 48 positions per angle and normalized for the redundancy that is inherent in the sampling technique (*10*). Each detector position in the sorted

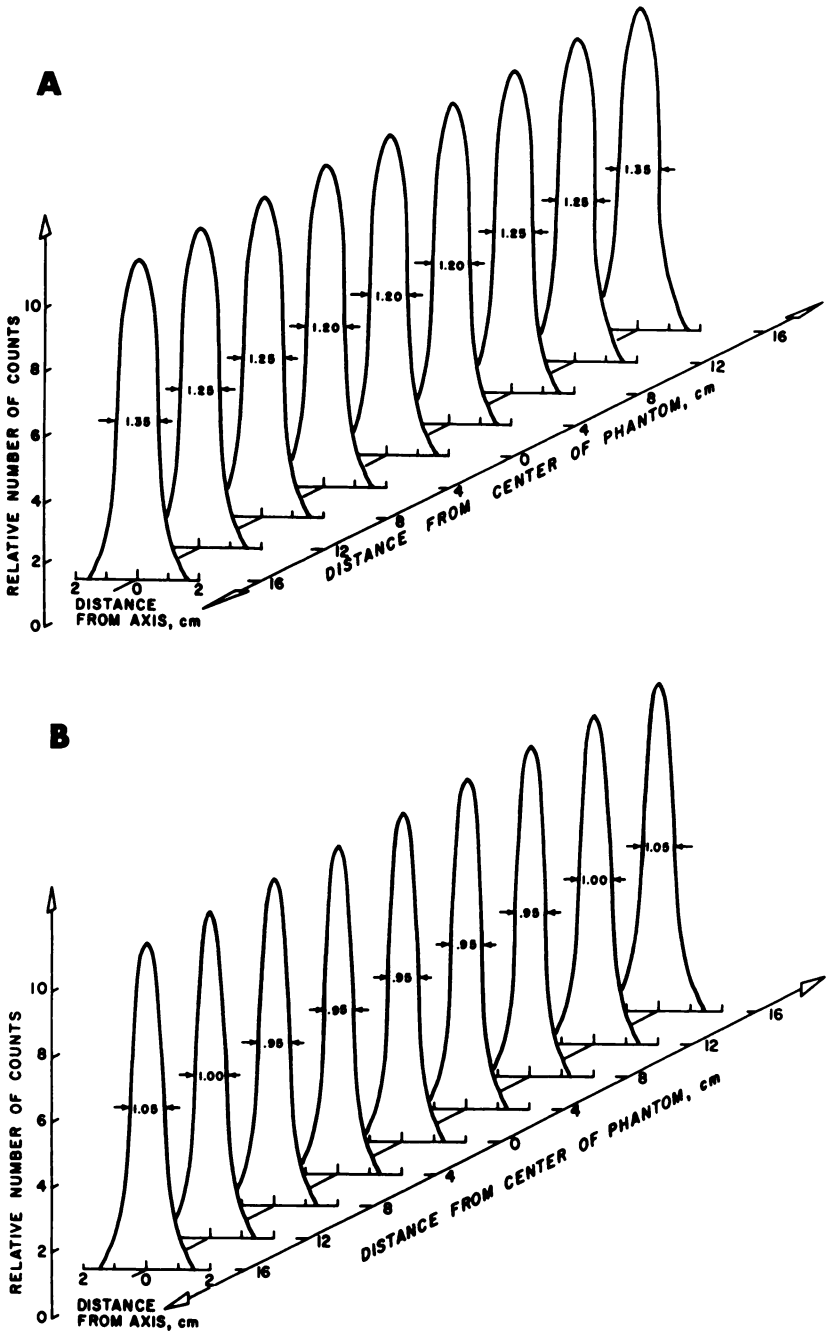

FIG. 4. Line spread functions for pair of NaI(Tl) crystals used in PETT III. Shadow shield is in place, only photopeak events were accepted, and measurements were taken as function of depth in water bath. (A) $\Psi = 0°$; (B) $\Psi = 21°$.

data is then multiplied by the corresponding coefficient from an attenuation correction array. These coefficients are either calculated from the average attenuation coefficient by assuming the cross section to be a homogeneous ellipse or they are measured with a standard source before performing the emission scan (*1,2*).

A 100 × 100 matrix is reconstructed in 60 sec from the set of 60 profiles, using a fixed-point convolution-based algorithm and one of several filter functions. The reconstruction algorithm, developed at the Biomedical Computer Laboratory at Washington University, permits optional decentering correction, sampling distance, and x,y origin. The image is displayed in 64 gray levels on a television monitor with a software-controlled variable window. Assembly-level programs or subroutines comprise approximately 60% of this software; the remainder is written in FORTRAN.

EVALUATION OF PETT III

Component evaluation. The initial evaluation of the system was done to test all the coincident detector pairs as rectilinear scanners and to evalute LSF

TABLE 3. VALUE OF Ψ AND FREQUENCY OF OCCURRENCE IN PETT III

Ideal angle (deg)	With shadow shield		Without shadow shield		Frequency of occurrence
	Photopeak only (deg)	100-keV discriminator (deg)	Photopeak only (deg)	100-keV discriminator (deg)	
0	0.0	0.0	0.0	0.0	8
3	3.1	3.1	2.9	2.9	14
6	6.2	6.2	5.9	5.9	12
9	9.3	9.3	8.8	8.9	10
12	12.4	12.5	11.9	11.8	8
15	15.4	15.4	14.8	14.7	6
18	18.2	18.3	17.5	17.4	4
21	20.6	21.1	20.1	20.0	2

distortion due to the angulation inherent in this multiple-coincidence scheme. The detectors and all shielding were placed in the relative positions they would occupy in PETT III. A ^{64}Cu line-source was moved about by a computer-controlled x,y positioning device. The LSFs were measured for all detector pairs with the source in a 20-cm-deep water bath which acted as a scattering medium.

The results of these measurements are partially summarized in Tables 1 and 2. The resolution of the various crystal pairs, given as the FWHM and Full Width at Tenth Maximum (FWTM) of the LSFs, were studied as a function of the angle Ψ formed by any pair of directly opposing detectors and the detector of interest on the opposite bank. Tables 1 and 2 list the results for the detectors with and without the shadow shields, respectively, for both the case in which only photopeak events are accepted and the case in which all events above 100 keV are accepted. These tables show the resolution to vary ±10% about a median value. This range is somewhat misleading in that detector pairs with large values of Ψ contribute much less to the image than those with small values of Ψ. Thus, the uniformity in overall image resolution is in fact better than indicated by Tables 1 and 2.

In Figs. 4A and 4B the LSFs for the two extreme values of Ψ (0° and 21°) are plotted as a function of the depth between detector pairs. Again, the variation in resolution with depth is about ±10% in any one line. The cases plotted in Fig. 4 are the most sensitive to Ψ and depth. The apparently anomalous narrowing of the LSFs for $\Psi > 0°$ is due to the fact that the line-source is viewed by the detector through a hole which is projected as an ellipse in the image plane. The loss in detection efficiency for $\Psi > 0°$ is the result of both this effect and the greater detector separations for these angles.

Complete sets of LSF data, as in Fig. 4, were taken for all Ψ with and without shadow shielding and for discriminator settings accepting photopeak events only and for settings accepting all events above 100 keV. These measurements were undertaken to evaluate how closely the assumed value of Ψ approximated its real value.

The errors in Ψ are the result of several factors:

1. The tangent of Ψ is not exactly proportional to Ψ, as was assumed, and that approximation becomes worse the larger the value of Ψ.
2. There are edge effects in the NaI(Tl) crystal that are not symmetric when $\Psi \neq 0°$, causing the apparent center of the detector to move.
3. The useful depth of the NaI(Tl) crystal varies with Ψ.

By measuring the actual value of Ψ between two crystals, the error due to these effects can be evaluated.

The centroid position of each LSF was calculated as a function of depth between all coincident detector pairs. A straight line was fitted to the centroid positions in the set of LSFs for each detector pair

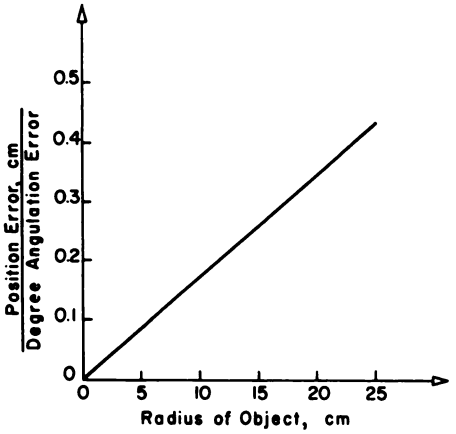

FIG. 5. Plot of error per degree of (Ψ) angulation error in placing line of response in image versus radius of object. Error is zero at center line and increases with distance from center line.

with a least-squares program, and Ψ was calculated for each pair using these lines. In Table 3, the ideal Ψ is listed in the first column, with the measured values of Ψ in the next four columns. The sixth column lists the relative contribution of each of these angles to the image. For those values of Ψ with the largest error (18° and 21°), the relative contribution to the image is quite small. In Fig. 5 the error in placing data in an image is plotted as a function of object size for a 1° error in Ψ. The error due to these angulation effects is zero at the center line between detector banks and increases with distance from the center line. Figure 5 and Table 3 show that the worst error would be when $\Psi = 21°$ for fully exposed crystals. The error would be 4 mm at the edge of a 46-cm-diam object. For all other values of Ψ, the error drops to less than 2 mm.

RESOLUTION

The loss of resolution due to the reconstruction algorithm, angulation errors, and detector motion was evaluated by taking an image of a line-source placed near the center of the field of view. A profile through the position of the line-source in the image gives a "LSF" for the reconstructed image. This measurement was obtained with the shadow shields in place with the lower level discriminator set at 100 keV. If the finite width of the inscribed square in a cylindrical line-source is subtracted, the net FWHM is 1.35 cm, which is only 1 mm more than the weighted average of 1.25 cm for the FWHMs of the LSFs of the individual detector pairs.

In order to evaluate the resolution in the presence of interfering sources and for various positions in the field of view, an image was taken with a multiple-line-source phantom. The phantom was a 20-cm Plexiglas disk, 6 cm deep, with 2-mm holes filled with a solution of a positron-emitter. The sources were spaced 2, 3, 4, and 5 cm apart on four sets of equally spaced radial lines. Figure 6 shows the image obtained with shadow shields in place and discriminator set at 100 keV. The FWHM of all sources was evaluated from a numerical printout of the image. This value was found to be about 13.8 ± 0.9 mm. Basically the resolution is that of the LSFs of the detector pairs, plus about 10% due to noise caused by the reconstruction and scanning processes.

Phantom studies. A uniformity phantom, consisting of a 25-cm-diam by 5-cm-deep Plexiglas container filled with a ^{68}Ga solution, was scanned with PETT III. The shadow shields were in place and the discriminators set at 100 keV. The resulting image is shown in Fig. 7. The distribution of the activity values per pixel in a 15-cm-diam central region of the image was used to evaluate their stand-

FIG. 6. Image of multiple-line-source phantom. The spacings on radial rows are 2, 3, 4, and 5 cm. Linear sampling was 0.5 cm; angular increments 3°. Shadow shields were in place and discriminators set at 100 keV. There are 4.8 million counts in image, which was obtained in 40 min at very low singles counting rate to avoid all problems due to randoms.

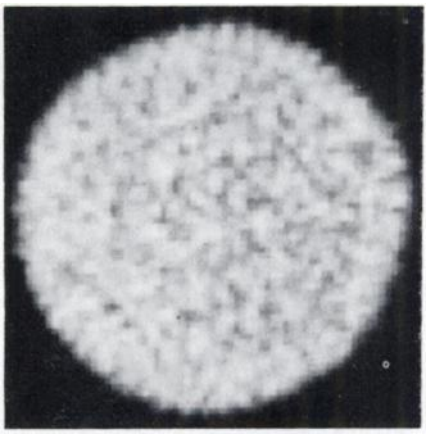

FIG. 7. Image of uniformity phantom containing 5 million counts. Image was obtained with shadow shields in place and with 0.5-cm linear sampling distance.

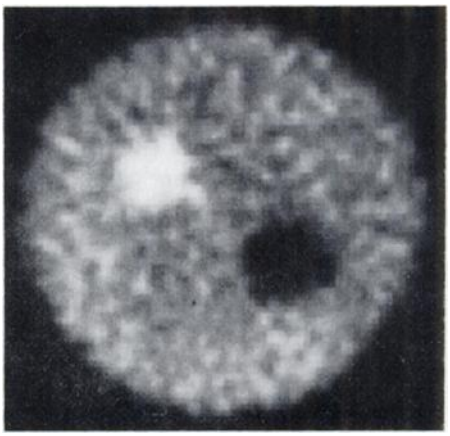

FIG. 8. Image of phantom shows quantitative recovery of activity distribution. Image (2 million counts) was taken with shadow shields in place and with 0.5-cm sampling distance. Body of phantom, hot spot, and void have relative activities of 1.0, 2.0, and 0.0. Values obtained in reconstructed image are in good agreement with these values.

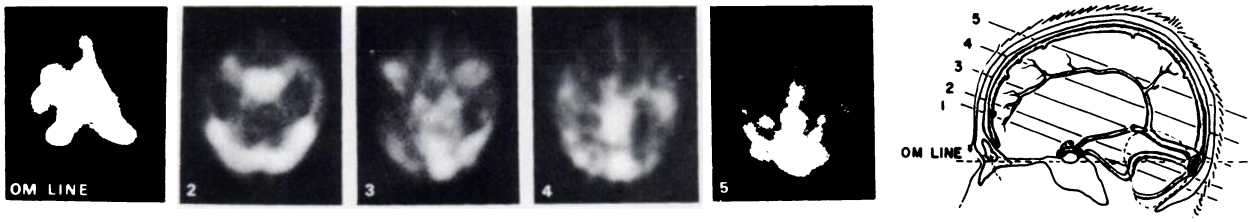

FIG. 9. Images of ^{11}CO-carboxyhemoglobin in brain. Positions of various slices are indicated in anatomic drawing. Images were obtained in 8–12 min with 300K to 800K counts. Shadow shields were in place.

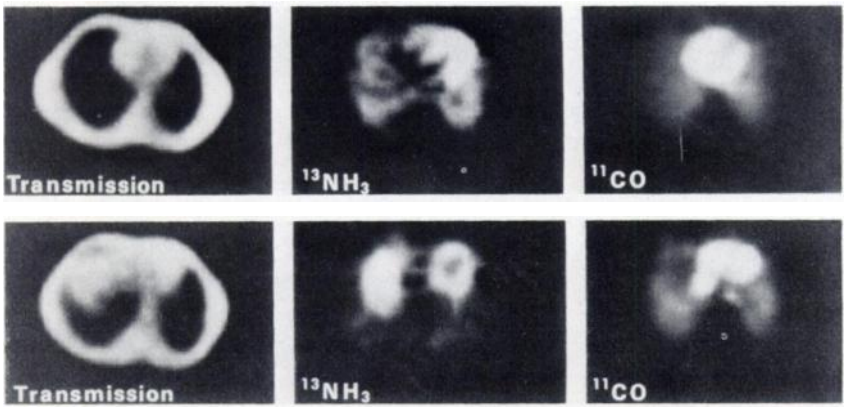

FIG. 10. Transmission, $^{13}NH_3$, and ^{11}CO-carboxyhemoglobin images taken at level of heart. Images were taken in 10–16 min with ECG gating for diastole and contain 210K to 570K counts. Shadow shields were in place.

ard deviation over the field in the reconstructed image: it was found to be ±7.5% of the mean value. The theoretical error (*11*) for this image, assuming only statistical error, is ±5.3%.

Another Plexiglas phantom, 20 cm in diameter with two 3.4-cm-diam tubes with relative activities of 1.0 in the main body and 0.0 and 2.0 in the tubes, was also imaged with the same procedure as that for the uniformity phantom (Fig. 8). This measurement was done to evaluate the quantitative recovery of information in a PETT III image. Within statistical error, the value of the hot spot in the reconstructed image is twice that of the main body, and the cold spot is zero.

Initial human studies. Initial studies with human subjects were done with normal volunteers. The studies were performed with $^{13}NH_3$ (*12*) and red cells labeled with ^{11}CO (*13*). The $^{13}NH_3$ was administered intravenously and the ^{11}CO was administered as a gas by rebreathing for 30 sec from a rebreathing bag. Patient studies also included ^{68}Ga-EDTA images; the ^{68}Ga-EDTA was obtained from a ^{68}Ge–^{68}Ga generator provided by New England Nuclear Corp.

The first organ of interest was the brain. Figure 9 shows a series of images of the blood pool after inhalation of 20 mCi of ^{11}CO. These images were obtained with the 2.5-cm shadow shields in place. The data collection periods ranged over 8–12 min with 300,000–800,000 counts per image. These images reflect the blood volume distribution of the brain. The images correlate well with normal human anatomy.

The next set of images was taken at the level of the heart, all with the 2.5-cm shadow shields in place and with ECG gating to include most of the diastolic phase. The transmission images (Fig. 10) locate the heart and, in the lower image, the liver. The left ventricle is prominent in both $^{13}NH_3$ images, with the right ventricle showing faintly. The ^{11}CO-hemoglobin images clearly delineate the chambers of the heart, confirm the identification of the right ventricle, and indicate the position of the right atrium and the aorta.

Images (Fig. 11) were also obtained in the upper abdomen. In the blood pool image the spleen is very prominent since ^{11}CO is a red cell tag. The $^{13}NH_3$ is taken up mainly by the liver.

Initial patient studies. A patient with a 2-week-old cerebral infarct was studied with $^{13}NH_3$, ^{11}CO, and ^{68}Ga-EDTA. The shadow shields were removed to maximize the counting rate. The patient was administered 8 mCi of $^{13}NH_3$, 3 mCi of ^{68}Ga-EDTA, and 20 mCi of ^{11}CO (by inhalation). The images required 8–20 min per slice (20 min for ^{68}Ga), with about 10^6 counts per image. The images are shown in Fig. 12 along with an EMI scan enhanced with radiographic contrast material. The infarct is promi-

nent in the $^{13}NH_3$ image, while the ^{68}Ga and EMI scans indicate abnormalities adjacent to the actual infarct due to impairment of the blood–brain barrier.

A patient with a highly vascular metastatic brain tumor was studied as above. Figure 13 shows the $^{13}NH_3$ and ^{68}Ga images. The tumor is prominent with both radiopharmaceuticals, in two levels. Additional PETT studies of both normal and abnormal volunteers can be found in Refs. *14* and *15*.

CONCLUSIONS

We have shown the imaging capability of positron-emission transaxial tomography, and PETT III in particular. The initial patient and volunteer studies show a great potential for imaging in a clinical situation.

The LSF and phantom studies show the high resolution capabilities of PETT III. The depth-independent resolution, quantitative recovery of radiopharmaceutical distributions, and removal of superposition of structures give PETT III advantages not present in conventional nuclear medicine imaging systems.

The PETT III has an added advantage in its flexibility. The design allows the sampling to be very fine or coarse as the situation dictates. As a result of the redundant sampling, it is possible to change the angular increments to 6, 12, or 15° for very rapid scanning and still have sampling every 3°. Other combinations of linear and angular sampling could allow very fine sampling. It is possible to change the resolution by changing shadow shields, and in about the same time that it takes to change a collimator on a scintillation camera.

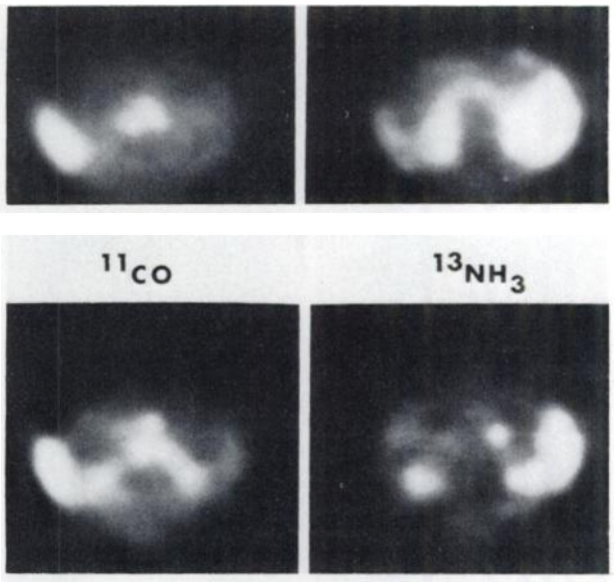

FIG. 11. Images in upper abdomen obtained with ^{11}CO and $^{13}NH_3$. Bottom is posterior. Both ^{11}CO images clearly show spleen, aorta, and vena cava. Lower ^{11}CO image also apparently shows left renal artery or vein and blood pool in kidney. Both $^{13}NH_3$ images show liver prominently and apparently both kidneys are also visible. These images were obtained in 6–12 min and contain 300K to 1800K counts per image. Shadow shields were in place.

We have shown that with one radiopharmaceutical, $^{13}NH_3$, it is possible to visualize with ease an abnormality, the cerebral infarct, that is particularly difficult to image by other methods. The radiopharmaceuticals that we have used to the present time are not very organ-specific, yet we have obtained high-quality images with reasonable scanning times and patient doses comparable to those used in

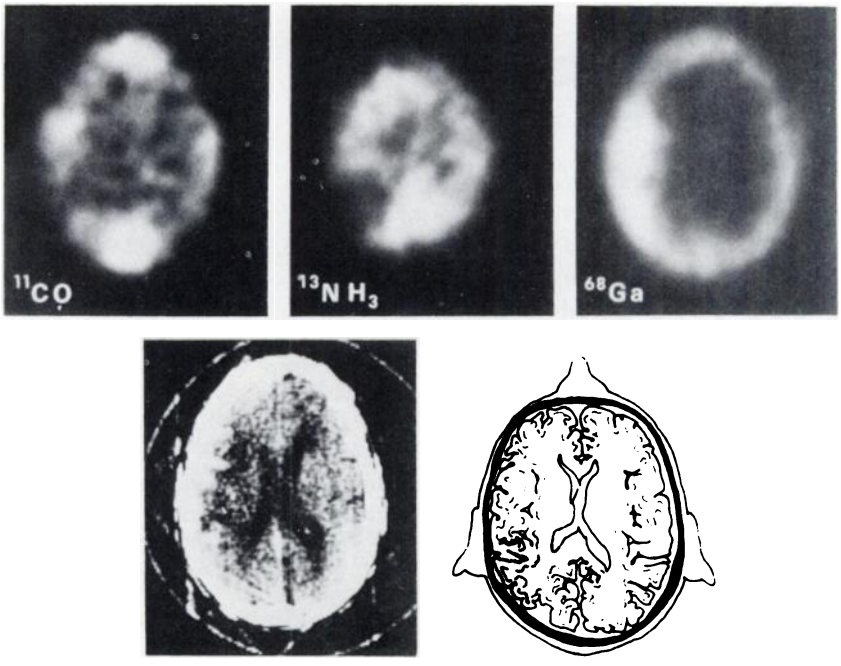

FIG. 12. Set of images of patient with large cerebral infarct. Shaded region in anatomic drawing indicates infarcted area. Both ^{11}CO-hemoglobin and $^{13}NH_3$ images clearly show regions of low perfusion, while ^{68}Ga-EDTA scan and EMI scan with contrast show only nearby regions of damage and do not show region of actual infarction. Shadow shields not used.

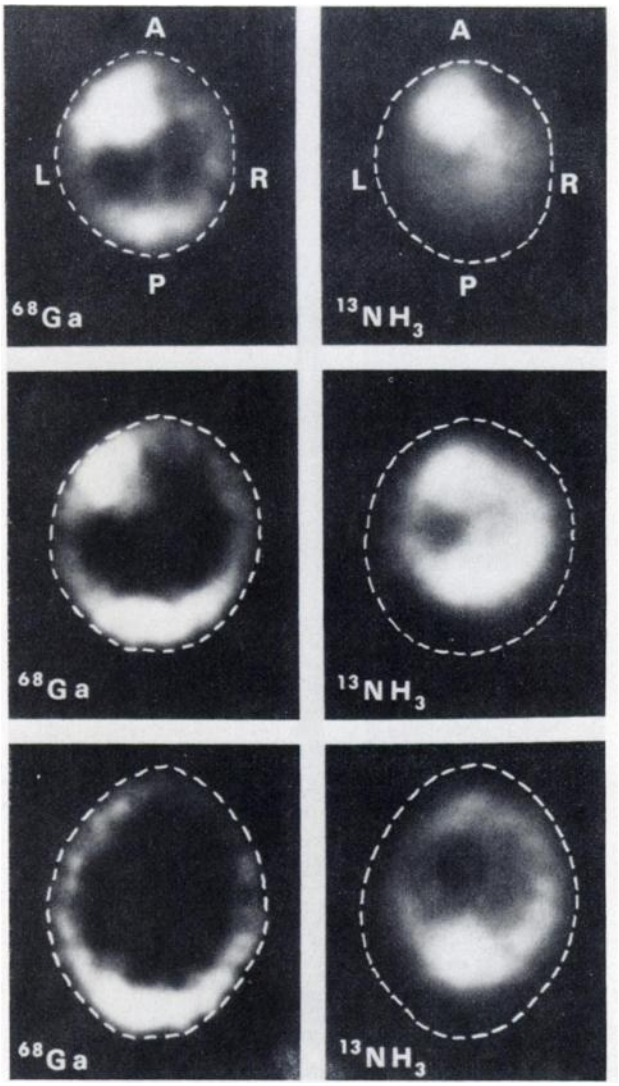

FIG. 13. Images of patient with highly vascular metastatic tumor. Dashed lines indicate approximate position of scalp. Tumor is prominent in upper two slices in $^{13}NH_3$ and ^{68}Ga-EDTA images, indicating both high perfusion and breakdown of blood–brain barrier. Shadow shields not used. (Top) 10 cm; (middle) 8 cm; (bottom) 6 cm above OM line.

present-day nuclear medicine techniques. With the development of better radiopharmaceuticals, the PETT III system should be able to give better images in shorter times at lower doses. With the choice of positron-emitting nuclides available, the number of compounds that could be labeled with a positron-emitter is virtually unlimited.

ACKNOWLEDGMENTS

We wish to thank J. R. Cox, D. Snyder, and H. Huang for the development of the reconstruction algorithm, J. Hood and J. Hecht for technical assistance in the design and construction of PETT III, R. E. Coleman, M. Raichle, R. Grubb, E. Weiss, and B. Sobel for helping to obtain patients and volunteers. We wish to thank M. J. Welch and M. G. Straatmann for developing and providing the radiopharmaceuticals. This work was supported by NIH Grants 5-P01-HL13851 and 1-R01-HL15423 and by NIH Fellowship 1-F03-GM55196-01.

REFERENCES

1. PHELPS ME, HOFFMAN EJ, MULLANI NA, et al: Application of annihilation coincidence detection to transaxial reconstruction tomography. *J Nucl Med* 16: 210–224, 1975

2. TER-POGOSSIAN MM, PHELPS ME, HOFFMAN EJ, et al: A positron emission transaxial tomograph for nuclear imaging (PETT). *Radiology* 114: 89–98, 1975

3. PHELPS ME, HOFFMAN EJ, HUANG SC, et al: Effect of positron range on spatial resolution. *J Nucl Med* 16: 649–652, 1975

4. PHELPS ME, HOFFMAN EJ, MULLANI NA, et al: Transaxial emission reconstruction tomography: Coincidence detection of positron-emitting radionuclides. In *Noninvasive Brain Imaging*, DeBlanc HJ, Sorenson JA, eds. New York, Society of Nuclear Medicine, 1975, pp 87–110

5. CHESLER DA: Three-dimensional activity distribution from multiple positron scintigraphs. *J Nucl Med* 12: 347–348, 1971

6. CHESLER DA: Positron tomography and three-dimensional reconstruction technique. In *Tomographic Imaging in Nuclear Medicine*, Freedman GS, ed. New York, Society of Nuclear Medicine, 1973, pp 176–183

7. ROBERTSON JS, MARR RB, ROSENBAUM M, et al: 32-crystal positron transverse section detector. In *Tomographic Imaging in Nuclear Medicine*, Freedman GS, ed. New York, Society of Nuclear Medicine, 1973, pp 142–153

8. CHESLER DA, HALES C, HNATOWICH DJ, et al: Three-dimensional reconstruction of lung perfusion image with positron detection. *J Nucl Med* 16: 80–82, 1975

9. CHO ZH, ERIKSSON L, CHAN J: A circular ring transverse axial positron camera. In *Reconstruction Tomography in Diagnostic Radiology and Nuclear Medicine, San Juan, April, 1975*, Ter-Pogossian MM, Phelps ME, Brownell GL, et al, eds. Baltimore, University Park Press: to be published

10. PHELPS ME, HOFFMAN EJ, COBLE CS, et al: Performance analysis of PETT III. In *Reconstruction Tomography in Diagnostic Radiology and Nuclear Medicine, San Juan, April, 1975*, Ter-Pogossian MM, Phelps ME, Brownell GL, et al, eds. Baltimore, University Park Press: to be published

11. HUANG H: Private communication, January 1975

12. STRAATMANN MG, WELCH MJ: Enzymatic synthesis of nitrogen-13 labeled amino acids. *Radiat Res* 56: 48–56, 1973

13. WELCH MJ, TER-POGOSSIAN MM: Preparation of short half-lived gases for medical studies. *Radiat Res* 36: 580–587, 1968

14. TER-POGOSSIAN MM, PHELPS ME, HOFFMAN EJ, et al: A positron emission transverse tomograph (PETT) for the three-dimensional and non-invasive measure of cerebral hemodynamics and metabolism. In *Proceedings of the Seventh International Symposium on Cerebral Circulation and Metabolism, Aviemore, Scotland, June, 1975*: to be published

15. TER-POGOSSIAN MM, HOFFMAN EJ, WEISS ES, et al: Positron emission reconstruction tomography for the assessment of regional myocardial metabolism by the administration of substrates labeled with cyclotron-produced radionuclide. In *Conference on Cardiovascular Imaging and Image Processing: Ultrasound, Angiography and Isotopes, July, 1975, Stanford University, Stanford, California*: to be published